An Investigation of Rotating Stall in a Single Stage Axial Compressor

STEPHEN R. MONTGOMERY
LIEUTENANT JOSEPH J. BRAUN, U. S. N.

REPORT NO. 29

GAS TURBINE LABORATORY
MASSACHUSETTS INSTITUTE OF TECHNOLOGY
CAMBRIDGE · 39 · MASSACHUSETTS

AN INVESTIGATION OF ROTATING STALL IN A SINGLE STAGE AXIAL COMPRESSOR

S. R. Montgomery
Lt. J. J. Braun, U.S.N.

National Advisory Committee for Aeronautics
Contract NAw - 6375
D.I.C. 7242
Gas Turbine Laboratory Report No. 29
May 1955

Massachusetts Institute of Technology

ABSTRACT

The rotating stall characteristics of a single stage axial flow compressor were investigated. The number of stall cells and their propagation velocities were found with and without stator blades. The measured velocities were compared wtih those predicted by Stenning's theory, assuming the downstream pressure fluctuations to be negligible, and correlation within 25% was obtained over a wide range of stall patterns. It was found that the pressure fluctuations caused by rotating stall were less downstream of the rotor than upstream; the minimum reduction across the rotor was 40% with stator blades, and 75% without stator blades. It was also found that, for the compressor tested, the stator blades decreased the number of stall cells and tended to induce rotating stall at larger mass flow rates.

1. Introduction

Rotating stall may be defined as a region of separated flow, moving relative to a blade row. It has been a continuing problem in axial compressor development since the resulting vibrations cause severe blade stresses to be imposed at low mass flow operation. If stall frequencies were predictable, blades could be designed having critical frequencies away from the stall frequency.

Several theories have been put forward for predicting the propagation velocity of a stall cell (References 1,2,3). These are all linearized analyses, with Sears and Marble considering the cascade as an actuator disc, and Stenning a cascade of finite width. A further difference in the theories occurs in connection with the assumption of the downstream flow field; Sears and Marble considered the wakes to mix in zero length, so that the flow field is a continuum, while Stenning also considered the alternative assumption of a series of free jets discharging into a region of constant pressure.

Experimental work has already been conducted on compressors, in particular at Harvard, California Institute of Technology and the N.A.C.A. (References 4,5,6). However, in each instance the work has been carried out on multi-row machines, and it appears that considerable interference results from the downstream blade rows.

Since the theories are in variance, and the interference due to other blade rows has an unknown effect, the present investigation has been conducted on a single stage machine, with and without stator blades, in an effort to verify the predicted results with a minimum of interference. The data obtained permit a ready comparison between predicted and actual stall propagation velocities, in addition to allowing the theoretical models for the downstream flow field to be checked by measurement of the pressure fluctuations.

2. Equipment and Procedure

2.1 Equipment

The single stage compressor used in these tests is shown in Figures 1 and 2. It has three blade rows; inlet guide vanes, rotor and stator, each of "free vortex" design. The characteristics of this compressor are presented in Reference 7.

The compressor geometry is:

Outside radius	11.625"
Hub-tip ratio	0.75
Blade chord length	1.5"
Blade aspect ratio	1.9
Pitch-chord ratio	0.95 at mean radius

Blade tip clearance was approximately .035".

Blade angles in degrees measured from the axial direction are:

Radius ratio r/r_t	Inlet Guide Vanes		Rotor		Stator	
	Inlet	Outlet	Inlet	Outlet	Inlet	Outlet
.75	0	28.5	34.8	-2.9	48.9	23.3
.80	0	27.1	38.0	7.1	47.2	22.0
.85	0	25.7	42.9	15.7	46.2	20.6
.90	0	24.4	47.5	23.4	45.1	19.4
.95	0	23.3	51.6	29.7	44.3	18.3
1.00	0	22.2	54.6	34.4	43.3	17.2

The blade profiles were NACA four digit series ten percent thick. Figure 3 is a sectional view of the blade region where velocity and pressure measurements were made. An adjustable throttling valve downstream of the blades permitted variation of mass flow.

Qualitative measurements of velocity fluctuations, used to indicate the stalled region, were obtained by the use of a constant current hot wire anemometer* The wire on the probes was tungsten, .00035" diameter and .044" long. An additional hot wire set, locally constructed, was also used when simultaneous indications at different tangential positions

---

* Model HWB, manufactured by Flow Corporation, Cambridge, Massachusetts.

were required. The operation of each set is identical and the same size probes were used for each.

The output of the hot wire anemometers was fed into a dual-beam cathode ray oscilloscope*, which permitted visual observation or photographic recording of the velocity fluctuations. Photographs were obtained with both a still and a strip film camera, the strip film camera being employed to include a greater number of stall cells on a single photograph. Representative photographs of each type appear as Figures 4 and 5. The time trace included on each velocity fluctuation photograph was obtained by feeding the output of an audio oscillator into the beam intensity control of the oscilloscope. The photographic and hot wire equipment is seen in Figure 1.

Pressure fluctuations were measured with a barium titanate crystal, the output of which was fed through an amplifier, and thence to the oscilloscope. The pressure taps were located in the outer casing of the compressor before and after each blade row and representative photographs of the pressure fluctuations at various axial positions are shown in Figures 6 and 7.

A five-hole probe and a sphere probe† were used to determine air angles and mean radius static pressure respectively. The description of these probes is given in Reference 8. The mass flow corresponding to each throttle position was obtained by measuring, with an inclined manometer, the total and static pressure in a calibrated nozzle.

2.2 Procedure

Runs were conducted at 1500 RPM, with and without stator blades. This rotational speed was chosen becuase it gave a maximum axial velocity of 90 feet per second, which satisfied the requirement for

---

* Type 322, manufactured by Dumont Laboratories, Inc., Clifton, New Jersey.

† Manufactured by Flow Corporation, Cambridge, Massachusetts.

incompressible flow. A few runs conducted at 60 percent higher speed indicated similar stall characteristics, so that the results obtained are representative for the machine over a range of rotational speeds. The various stall regions were obtained by varying the position of the throttle and thereby the mass flow. The change over from one stall region to another was quite sharp and easily detectable by sound and change in the velocity fluctuation pattern.

The data recorded in each run were static and total pressure in the calibrated nozzle, photographs of the velocity fluctuation pattern and photographs of the pressure fluctuations before and after the rotor and stator. The velocity fluctuations were normally measured at the mean radius, but radial traverses were made to detect any change from root to tip. These data permitted the evaluation of the frequency of the rotating stall, mass flow and relative magnitude of pressure fluctuations at the various axial positions.

The number of stalled regions was determined by the use of two hot wire probes, one stationary and one free to traverse tangentially. The wires were initially aligned so that the output signals were in phase and one wire was then traversed through a known arc. The relative phase displacement of the stalled region was then correlated with the tangential distance traversed to determine the number of stalled regions.

The rotor performance was obtained by measuring the static pressure and air angles at the mean radius, before and after the blade row, using the sphere and five-hole probes. The pressures were measured with an inclined manometer and data were obtained for mass flow rates varying from the maximum down to the point where the probe readings became meaningless due to large velocity fluctuations.

3. Results

The data were obtained in the form of the steady state characteristics of the compressor and photographic records from the hot wire equipment, and the results are presented in Figures 8 to 13. From measured values of axial velocity and inlet and outlet angles from the rotor at the mean radius, the angles relative to the rotor, β_1 and β_2, were calculated, using the relations

$$\tan \beta_1 = \frac{u}{c_x} - \tan \alpha_1$$

$$\tan \beta_2 = \frac{u}{c_x} - \tan \alpha_2$$

Figure 8

Hence, knowing the static pressure rise Δp_s measured at the mean radius, the pressure coefficients were calculated and plotted versus β_1.

$$C_p = \frac{\Delta p_s}{\frac{1}{2}\rho w_1^2}$$

Figure 9

Finally, the blockage coefficient α, as used by Stenning and Emmons (Reference 3,6) to analyze the stability of a propagating wave, was calculated and plotted versus cotangent β_1 :

$$\alpha \approx \frac{A}{A_1} = \frac{\cos \beta_1}{\cos \beta_2 \sqrt{1-C_p}}$$

Figure 11

From the photograph of the hot wire traces, the frequency of stall propagation was found using the frequency of the timing pulse or the velocity of the film strip. The number of cells was found from the comparison of phase change with the actual angular displacement of the two probes used, and hence the absolute frequency of a single cell was calculated. Taking the mean radial position as the point of reference, the velocity V of a single cell relative to the rotor can be calculated and is plotted, non-dimensionally, as V/c_x versus β_1 in Figures 12 and 13.

In addition, the theoretical propagation velocities can be calculated from the theories of Marble, Sears and Stenning. The first two

give an identical result:

$$\frac{V}{c_x} = \csc 2\beta_1$$

The third theory includes an effect due to the number of stall cells, N, and gives the result:

$$\frac{V}{c_x} = \frac{2(1-C_p)}{\sin 2\beta_1 \left\{ \frac{L\pi}{b \cos\beta_2} \left[\frac{1-e^{-2\pi p/b}}{1+e^{-2\pi p/b}} \right] + 1 \right\}}$$

where b is the half wavelength of one cell ($\frac{\text{circumference}}{2N}$), L is the chord length and p is the separation between the rotor and inlet guide vanes; the expression in the square brackets is a correction designed to allow for the effect of the inlet guide vanes on the stall propagation velocity. These theoretical velocities were calculated from the steady state characteristics of the compressor, and are plotted in Figures 12 and 13.

4. Discussion of Results

4.1 Steady State Characteristics

The steady state characteristics were obtained both with and without the stator blades in position, and excellent agreement was obtained between the observed data. In addition, it was found that, without the stator blades, it was possible to obtain reasonable data when stall cells of short wave length were present, so that mean data are available for part of the region of rotating stall.

In Figures 9 and 10, where the pressure coefficient is plotted versus β_1, the ranges in which rotating stall occurs are marked both for the stage with stator blades and for that without; a detailed discussion of these regions is given below. It will be noted that there is a rise in pressure coefficient at a value of β_1 of 66°. This was due to the onset of rotating stall, which caused the flow through the stalled blade passages to decrease, while the flow through the unstalled blade passages increased. The net losses across the blade row are apparently reduced, giving an increase in the pressure rise, and hence a local rise in pressure coefficient. With stator blades in place no reliable measurement of angles or static pressures are possible when stall begins, since the velocity fluctuations are large.

From stability considerations for a wave propagating in a cascade (References 3,6) the start of rotating stall is predicted to coincide with the point where a line from the origin is tangent to the curve of the blockage coefficient α versus cotangent β_1. In Figure 11, it is seen that stall propagation does not start until a somewhat larger value of β_1 than that predicted. This is probably due to the fact that finite fluctuations are involved, rather than the small fluctuations assumed in the theoretical model.

4.2 Stall Characteristics with Stator Blades

The first tests were conducted with the stator blades in position, and the following characteristics were observed as the relative inlet angle was increased by decreasing the mass rate of flow.

Four separate regimes of rotating stall were found, the first consisting of one cell at the tips of the blades, and the others having one,

two and three cells respectively, covering the entire blade. Between each regime, a transition state occurred in which the number of cells varied between those found in the adjacent regimes (Figure 9), The velocity fluctuations were measured at a number of axial positions, and it was found that the magnitude of the velocity fluctuations decreased with distance both upstream and downstream of the rotor.

The first sign of stall as β_1 was increased above the design value was the appearance of random velocity fluctuations, which appeared with increasing regularity until the regime of propagating tip stall was entered. The stalled region extended from the rotor tip for about 3/4 inches down the blade, a distance approximately equal to the thickness of the boundary layer entering the rotor (Reference 7). The number of blades over which the region extended was greatest at the tip and decreased further down the blade, but no actual measurements were made of the number of blades covered by the cell. As β_1 was further increased, a single cell was found extending over the entire blade length, and the number of blades covered increased with β_1 until the next regime with two stall cells was entered. In the regimes where the entire blade was stalled, neither the velocity fluctuation pattern, nor the number of blades covered, varied markedly from root to tip. As β_1 was increased, the number of cells increased progressively from one to two to three, a larger number being unobtainable as purely random fluctuations appeared when β_1 was greater than 81°, as shown in Figure 4-d.

4.3 Stall Characteristics Without Stator Blades

When the stator blades were removed, there was a very marked change in the rotating stall characteristics; the onset of stall was delayed until a greater value of β_1 and following the initial regime with random velocity fluctuations, two regimes were found consisting of a much larger number (eight and nine respectively) of small cells than were obtained with the stator blades in place. On further increase of β_1, the stall characteristics resembled those with the stator blades in place and regimes containing one, three and four cells were found before random stall reappeared at a value of β_1 of 85°. The regime with two cells

appeared as an unstable condition in a very narrow range of inlet angles. (Figure 10).

Several striking differences were observed between cells of short and long wavelength (high and low frequency). With the former, it was found that the velocity fluctuations were very nearly damped out in the root boundary layer, while the latter showed fluctuations of greater amplitude in the same place. It was also found that for short wavelengths, the velocity fluctuations measured directly downstream of the rotor (Section F, Figure 3) were considerably smaller than those at Section G. No satisfactory explanation of this has been suggested.

The limits of the various regimes were comparatively well defined when there were a small number of cells, since any change in number caused an appreciable change in the frequency, and in the phase shift between two probes. With eight or nine cells, the problem of determining the actual number becomes more difficult and there is a range of uncertainty between these two regions. Further difficulties are caused by the non-symmetry of the cells around the annulus (Figure 5), and also by the fact that each cell does not cause the same velocity fluctuations at the probe.

Since the blade passages are of finite width, the probe may be at any point across the passage at the instant when the adjacent blade stalls. The process of stalling causes separation from the leading edge of the blade, and there is a reduction of velocity in this region of separated flow (Position A), while the velocity in the unseparated portion of the passage may have an instantaneous increase, due to the reduction in flow area (Position B).

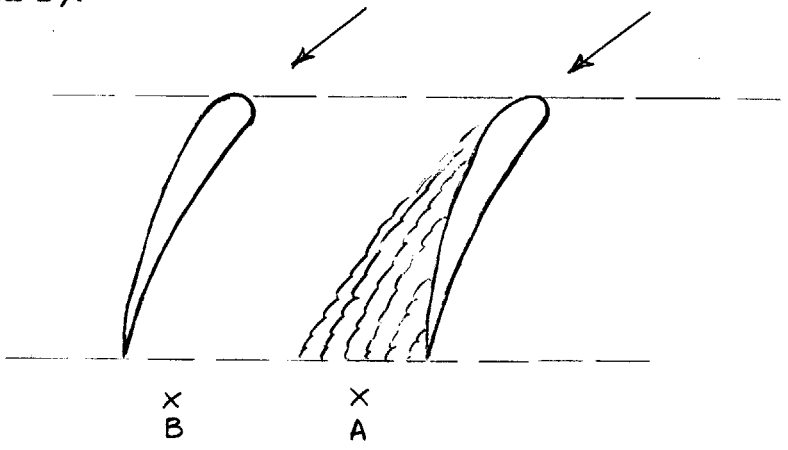

If the probe is close to the trailing edge of the blade, it may therefore show either an increase or decrease in velocity when stall occurs. Further downstream, mixing has occurred so that each stall cell causes a net decrease in velocity, and similarly, a probe upstream of the blade row will always indicate a reduction in velocity on account of the partial blockage of the blade passage. The phenomenon was noted for stall cells of short wavelength and would be expected when there are only a small number of blade passages covered by each cell.

Finally, it should be noted that a flow reversal will be shown as a velocity increase since a hot wire is non-directional, and hence the mid-point of the cell is sometimes difficult to find on the oscillogram.

4.4 Comparison of Actual and Predicted Propagation Velocities

As explained above (in Section 3), the experimental points and theoretical curves are plotted in Figures 12 and 13. The form in which these figures are presented permits a comparison of the theoretical and experimental values of the propagation velocities relative to the rotor, and important conclusions can be drawn from them.

First, all the theories are based on the assumption of small perturbations on a steady velocity field and so would only be valid at the onset of rotating stall. Good agreement is obtained at this point with Stenning's theory, both with and without stator blades, while the propagation velocities predicted by both Sears and Marble lie below the values observed with stator blades and above those observed without stator blades. At high values of the inlet angle, the velocity fluctuations cannot be considered as small, but all theories give the correct order of magnitude (within about 25%) for the propagation velocities if the theoretical curves are extrapolated. It will be noted that throughout the range of available data, the velocities predicted by Sears and Marble correspond almost exactly with those predicted by Stenning for four stall cells.

Another striking factor, without stator blades, is the sudden change from nine cells to a single cell, with a very small change in β_1 (Figure 13). The propagation velocity increases by ninety percent when this happens,

which would seem to confirm the prediction of Stenning's theory that the propagation velocity is a function of the number of cells and increases with increase of wavelength.

4.5 Pressure Fluctuations

In the theoretical analysis of rotating stall, two simple assumptions can be made about the conditions downstream of the blade row. Either the blade passages can be considered as nozzles discharging into a region of constant pressure, or it can be assumed that mixing occurs immediately downstream of the row, so that the downstream flow field is a continuum. These assumptions can readily be checked by measuring the relative magnitude of the upstream and downstream pressure fluctuations and the results of such tests, taken at the outer casing of the compressor, were as follows.

With stator blades in position, it was found that pressure fluctuations were negligible downstream of the stator blades and upstream of the inlet guide vanes, as compared with the fluctuations upstream of the rotor. The fluctuations downstream of the rotor were not greatly affected by the onset of rotating stall but in the extreme condition an appreciable variation is seen (Figure 6c). The upstream fluctuations due to rotating stall were approximately double those downstream of the rotor. It would appear from this that the condition of a constant downstream pressure field, as assumed by Stenning, was not satisfied and therefore the close agreement between theoretical and observed propagation velocities must be considered fortuitous.

Without stator blades, a greater reduction in pressure fluctuations across the rotor was found, as seen in Figure 7, and the maximum downstream fluctuations due to rotating stall were less than 25% of those upstream.

In order to confirm the most suitable assumption for the downstream flow field in the theoretical analyses, an expression for the magnitude of the pressure fluctuations, based on Stenning's model of the stall process with the downstream flow field considered as a continuum, is calculated in Appendix I. The expression obtained is:

$$\frac{\delta p_1}{\delta p_2} = \sqrt{\left\{1 - \frac{\tan \beta_1}{V/c_x}\right\}^2 + \left\{\left(\frac{1 - e^{-2\pi p/b}}{1 + e^{-2\pi p/b}}\right) \cdot \frac{1}{V/c_x}\right\}^2}$$

From experimental data on the propagation velocities of stall cells without stator blades, the predicted relative magnitude of the pressure fluctuations can be calculated and representative results are given in the following table.

Number of cells	8	9	1	3
β_1	67.0°	73.6°	74.6	78.5
$\tan \beta_1$	2.36	3.40	3.63	4.92
V/c_x	.862	1.24	2.32	2.54
$\frac{1 - e^{-2\pi b/a}}{1 + e^{-2\pi b/a}}$	.825	.867	.151	.413
$\delta p_1/\delta p_2$	1.99	1.88	0.56	0.96

From the observed values of pressure fluctuations without stator blades, it is seen that the ratio of pressure fluctuations is never less than four, so that the assumption of a constant pressure field downstream corresponds more closely to the observed results than the assumption of a continuum.

5. Conclusions and Suggestions for Future Work

From the results obtained, it can be seen that the propagation velocities can be predicted with reasonable accuracy for a single blade row at the onset of stall using the results of Stenning's theory. At high inlet angles relative to the rotor, where the velocity fluctuations become large and the pressure coefficient is small, the actual and predicted velocities agree reasonably well both with Stenning's theory, and with the results of Sears' and Marble's analyses. The correlation with the latter theories is probably somewhat fortuitous, as it is due to a cancellation of the effects of two invalid assumptions; namely, that there is a small pressure rise across the blade row, and that the downstream flow field can be represented by a continuum.

It is also seen that the rotating stall characteristics of the compressor are influenced very strongly by stator blades downstream of the rotor, the effect of this interference being to damp out the propagation of stall cells at high frequencies and to induce stall propagation at higher mass flow rates.

Finally, measurements of pressure fluctuations upstream and downstream of the rotor confirm that, for a single blade row, the assumption of a constant pressure field downstream is closer to the observed results than the assumption of a continuum.

It is proposed to continue work on the compressor using a single rotor, so as to eliminate completely the effects of adjacent blade rows, and new blades have been designed for such a rotor. By varying the stagger and solidity of these blades the effects of these parameters will be found and following this, stator blades will be installed in order to find their effect on the stall characteristics when the spacing between blade rows is varied.

APPENDIX I

AI.1 Pressure Fluctuations in a Downstream Continuum

The following analysis is designed to estimate the relative magnitude of the upstream and downstream pressure fluctuations caused by rotating stall when the downstream flow field is considered as a continuum.

The analysis is based on the model used by Stenning (Reference 3) shown in the following figure.

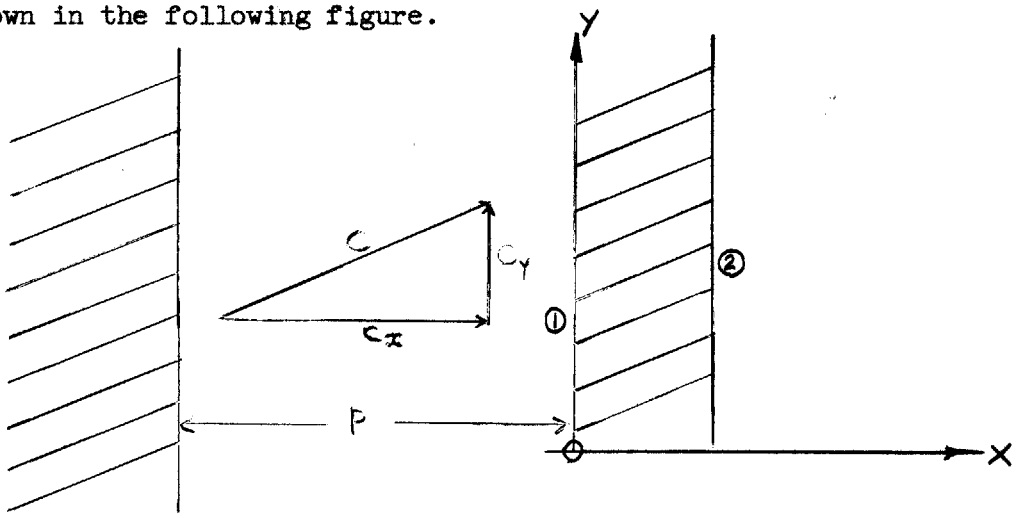

For incompressible, irrotational flow upstream, a perturbation velocity potential ϕ can be defined, and from continuity:

$$\phi_{xx} + \phi_{yy} = 0$$

If the rotating stall is considered as a sine wave propagating along the cascade, the solution is:

$$\phi = A \sin\left(\frac{\pi y}{s} - \omega t\right)\left[e^{\frac{\pi x}{s}} + e^{-\frac{2\pi}{s}(x+2p)}\right] \qquad (1)$$

which satisfies the condition that $\phi_x = 0$ at $x = -p$. This condition allows the interference effect due to upstream guide vanes to be estimated, on the assumption that these guide vanes are closely spaced and of large chord length.

From Euler's equations of motion for unsteady flow, with small perturbations, upstream of the cascade

$$\phi_t + c\,\delta c + \frac{\delta p}{\rho} = c \qquad -\infty < x < 0 \qquad (2)$$

Equation 2; Reference 3.

Downstream a continuum is assumed (Appendix III, Reference 3) and

$$\frac{\delta p_2}{\rho} = (\phi_t)_1 \tag{3}$$

By definition

$$c^2 = u^2 + v^2$$

$$\therefore c\,\delta c = u\,\delta u + v\,\delta v$$

$$\therefore c_1\,\delta c_1 = [c_x \phi_x]_1 + [c_y \phi_y]_1$$

Evaluating equation (2) at point 1 and dividing by equation (3)

$$\frac{\delta p_1}{\delta p_2} = \frac{-(\phi_t)_1 - c_1\,\delta c_1}{(\phi_t)_1} = \frac{-(\phi_t)_1 - [c_x \phi_x]_1 - [c_y \phi_y]_1}{(\phi_t)_1}$$

Substituting for ϕ from equation (1)

$$\frac{\delta p_1}{\delta p_2} = \frac{\left(1+e^{-\frac{2\pi b}{b}}\right)\left(\omega - \frac{\pi c_y}{b}\right)\cos\left(\frac{\pi y}{b} - \omega t\right) - \left(1-e^{-\frac{2\pi b}{b}}\right)\frac{\pi c_x}{b}\sin\left(\frac{\pi y}{b} - \omega t\right)}{\left(1+e^{-\frac{2\pi b}{b}}\right)\omega\cos\left(\frac{\pi y}{b} - \omega t\right)}$$

Comparing the magnitude of these pressure fluctuations,

$$\left|\frac{\delta p_1}{\delta p_2}\right| = \frac{\sqrt{\left(1+e^{-\frac{2\pi b}{b}}\right)^2\left(\omega - \frac{\pi c_y}{b}\right)^2 + \left(1-e^{-\frac{2\pi b}{b}}\right)^2\left(\frac{\pi c_x}{b}\right)^2}}{\omega\left(1+e^{-\frac{2\pi b}{b}}\right)}$$

$$= \sqrt{\left(1 - \frac{\pi c_y}{b\omega}\right)^2 + \left(\frac{1-e^{-\frac{2\pi b}{b}}}{1+e^{-\frac{2\pi b}{b}}}\right)^2\left(\frac{\pi c_x}{b\omega}\right)^2}$$

$$= \sqrt{\left(1 - \frac{\tan\beta_1}{V_{c_x}}\right)^2 + \left(\frac{1-e^{-\frac{2\pi b}{b}}}{1+e^{-\frac{2\pi b}{b}}}\right)^2\left(\frac{1}{V_{c_x}}\right)^2}$$

This equation shows that the effect of inlet guide vanes is to reduce the ratio of upstream to downstream pressure fluctuations, and it can be used to estimate the theoretical pressure fluctuations with the downstream flow field considered as a continuum.

NOMENCLATURE

A	Effective blade passage area
A'	Total blade passage area
b	Half wave length of stall cell
c	Resultant velocity
C_p	Pressure coefficient
	Axial velocity
	Tangential velocity
f	Stall propagation frequency
F	Frequency of timing pulse on photographs
L	Blade chord length
N	Number of stall cells
p	Separation between inlet guide vanes and rotor
p_s	Static pressure
r	Radius
r_t	Rotor tip radius
U	Rotor velocity at mean radius
V	Stall propagation velocity at mean radius
w	Inlet velocity relative to rotor
α	Blockage coefficient
α_1	Absolute air angle entering rotor
α_2	Absolute air angle leaving rotor
β_1	Air inlet angle relative to rotor
β_2	Air outlet angle relative to rotor
ρ	Density
ϕ	Perturbation velocity potential
ϕ_x	$\frac{\partial \Phi}{\partial x}$
ϕ_y	$\frac{\partial \Phi}{\partial Y}$
ϕ_t	$\frac{\partial \Phi}{\partial t}$
ω	Angular frequency of stall propagation

REFERENCES

1. Sears, W.R., "A Theory of Rotating Stall in Axial Flow Compressors", Cornell University, January 1953.

2. Marble, F.E., "Propagation of Stall in a Compressor Blade Row", Guggenheim Jet Propulsion Centre, California Institute of Technology, Technical Report 4, January 1954.

3. Stenning, A.H., "Stall Propagation in Axial Compressors", M.I.T. Gas Turbine Laboratory, Report 28, April 1955.

4. Emmons, H.W., Pearson, C.E. and Grant, H.P., "Compressor Surge and Stall Propagation", A.S.M.E. Annual Meeting, Paper No. 53-A-56, December 1953.

5. Iura, T. and Rannie,W.D., "Experimental Investigation of Rotating Stall in Axial Compressors", Transactions of the A.S.M.E., April 1954.

6. Huppert, M.C. and Benser, W.A.,"Some Stall and Surge Phenomena in Axial-Flow Compressors", Journal of the Aeronautical Sciences, December 1953.

7. Moore, R.W. and Schneider, K.H., "Measurement of Flow Through a Single-Stage Axial Compressor", M.I.T. Gas Turbine Laboratory, Report 27-6, December 1954.

8. Moore, R.W. et al., "Experimental Techniques for Three-Dimensional Flow Research", M.I.T. Gas Turbine Laboratory, Report 27-8, December 1954.

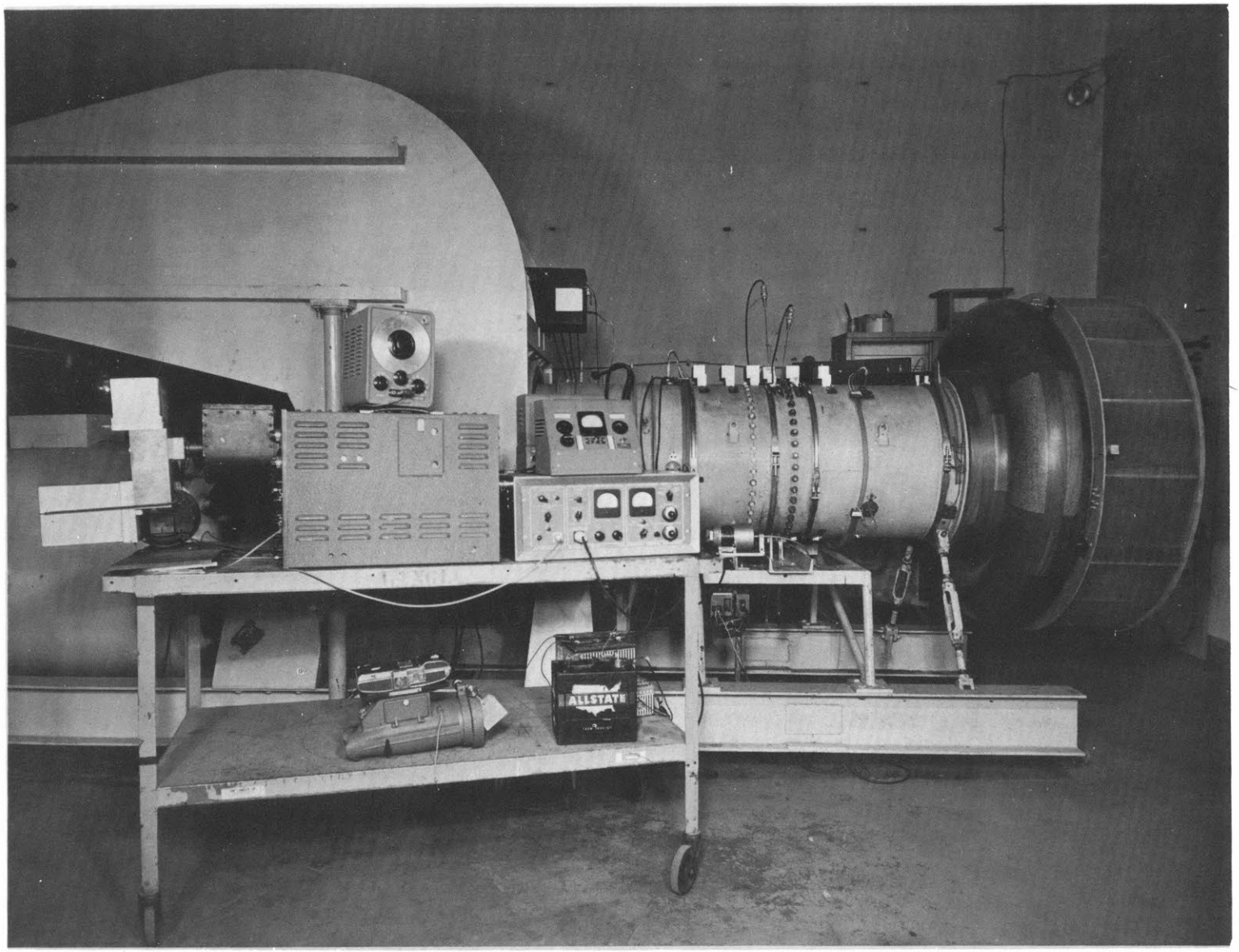

FIG. 1 PHOTOGRAPH OF APPARATUS

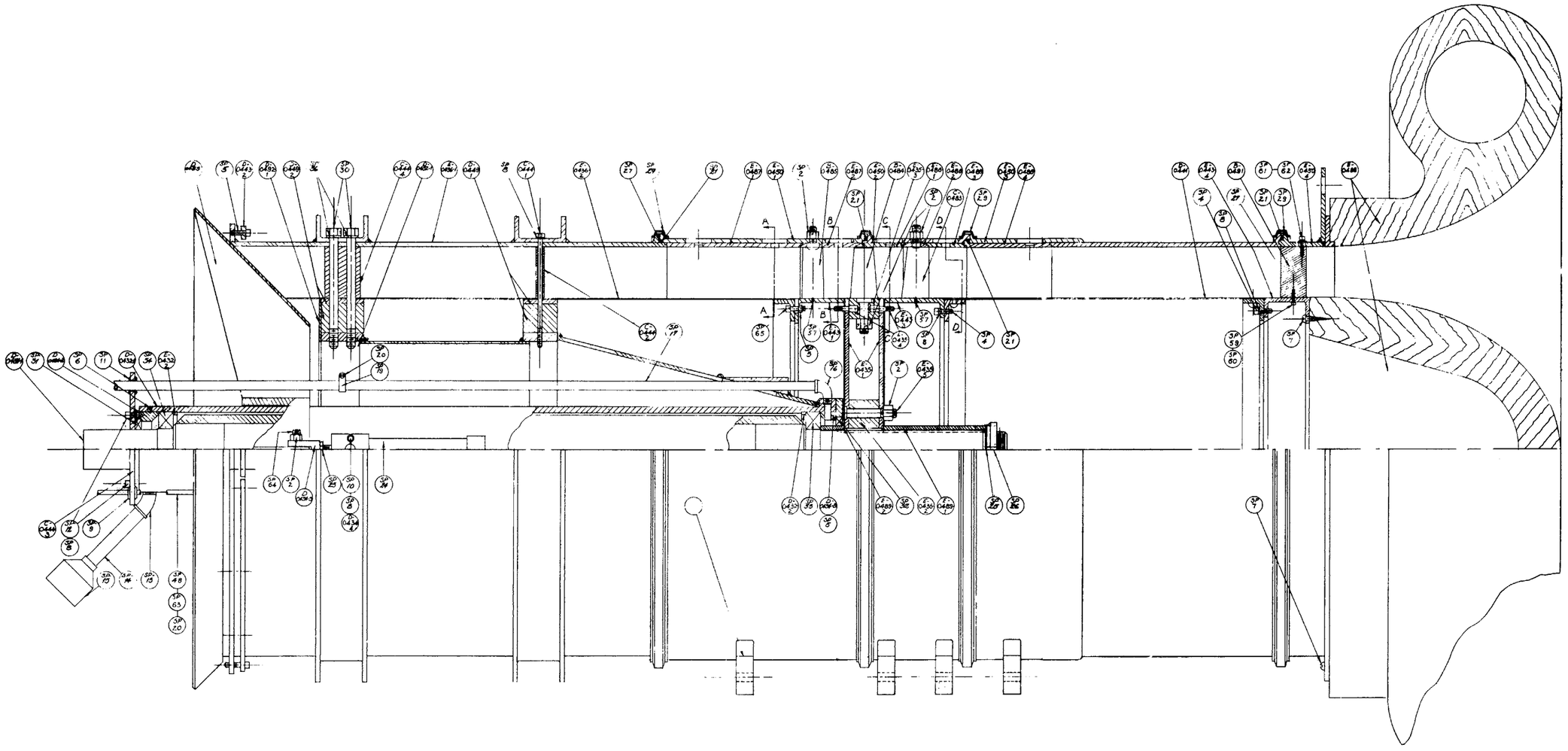

FIG. 2 - SECTIONAL DRAWING OF COMPRESSOR

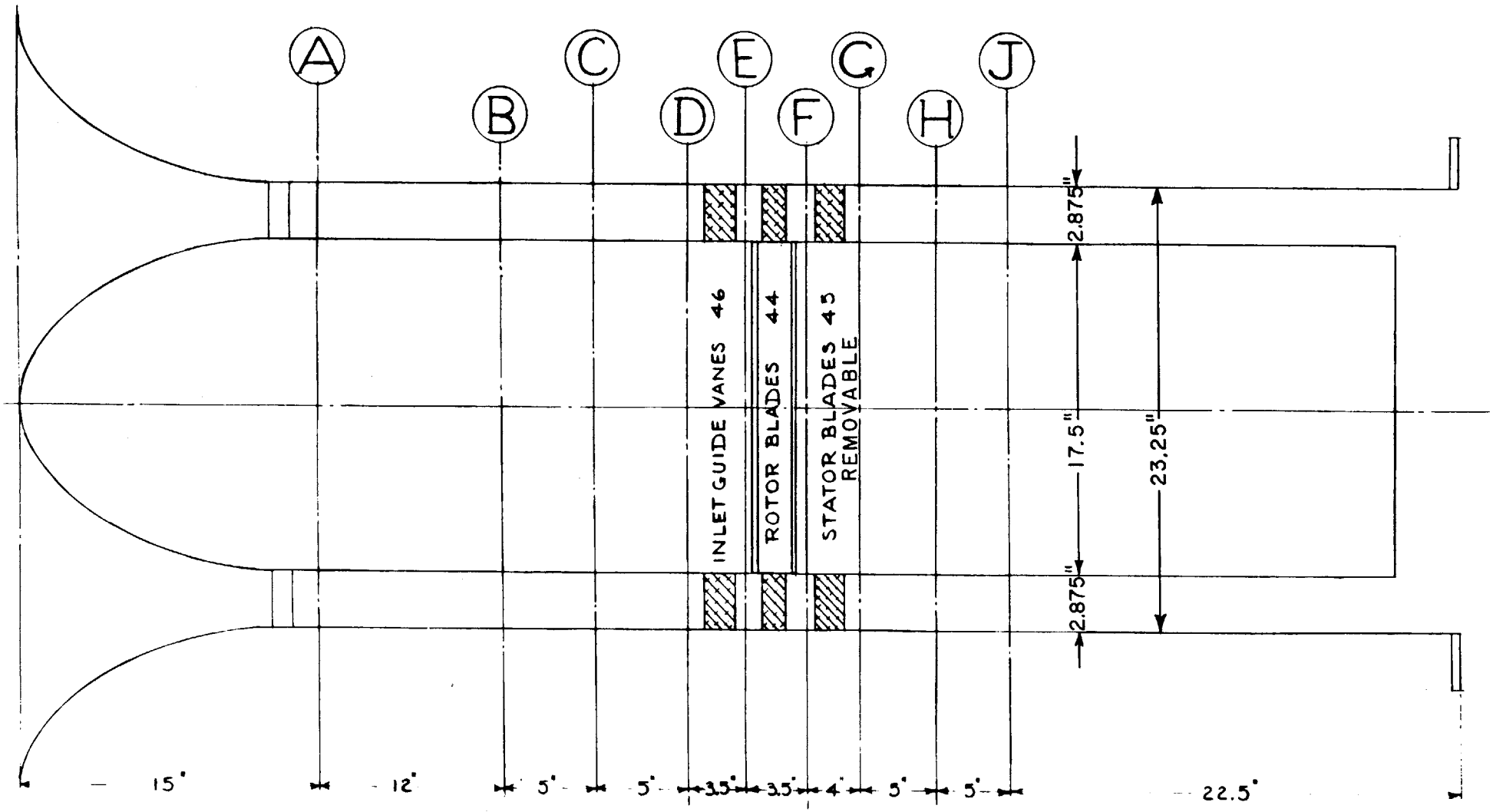

FIG. 3 - SCHEMATIC DIAGRAM OF MEASUREMENT STATIONS

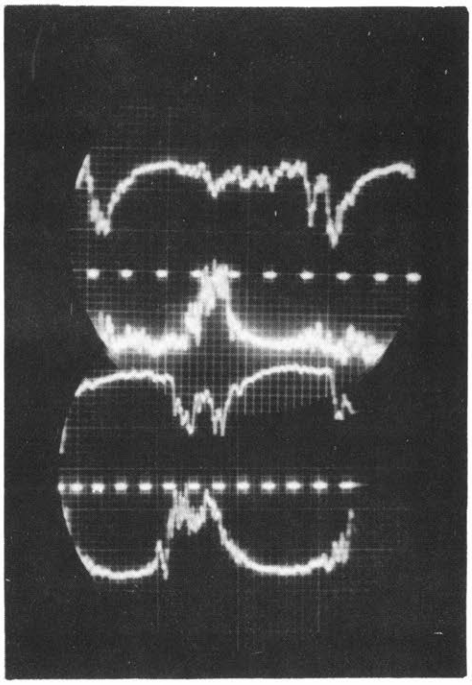

TIME ←

a. $B_1 = 63.0°$
F = 50 cps
N = 1 f = 7.85 cps

b. $B_1 = 67.9°$
F = 100 cps
N = 2 f = 15.5 cps

VELOCITIES DECREASE TOWARD THE CENTER OF EACH PICTURE
PROBES DOWNSTREAM OF STATOR
180° APART

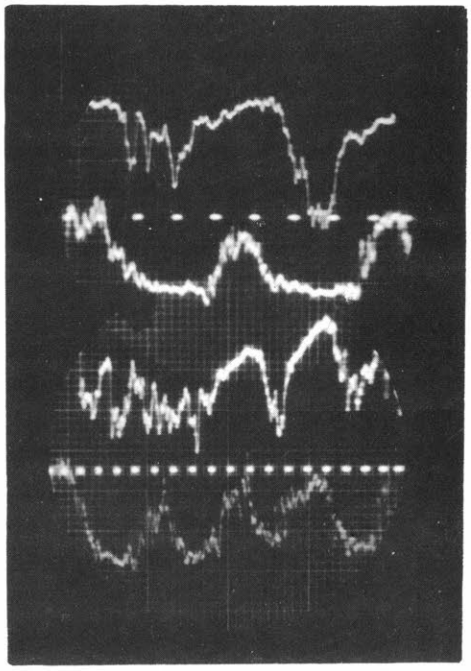

TIME ←

c. $B_1 = 73.8°$
F = 100 cps
N = 3 f = 23.2 cps

d. $B_1 = 80.6$
F = 100 cps

FIG 4. VELOCITY FLUCTUATIONS WITH STATOR BLADES

POSITIVE VELOCITY

NOTE: PROBES BEFORE ROTOR - WITH TWO PROBES, 45° APART, CLOCKWISE PROBE RECEIVES SIGNAL FIRST.

8 CELLS f = 135 CPS $\beta_1 = 67.0°$ 100 INS/SEC TIME

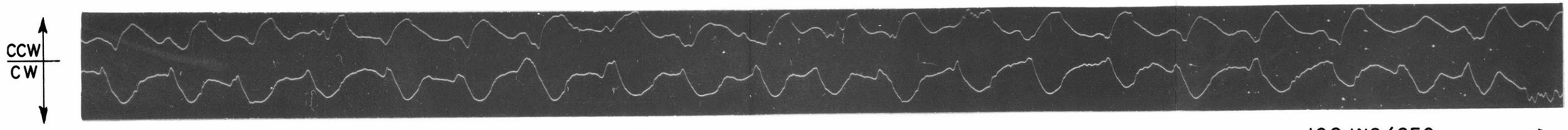

9 CELLS f = 149 CPS $\beta_1 = 73.6°$ 100 INS/SEC TIME

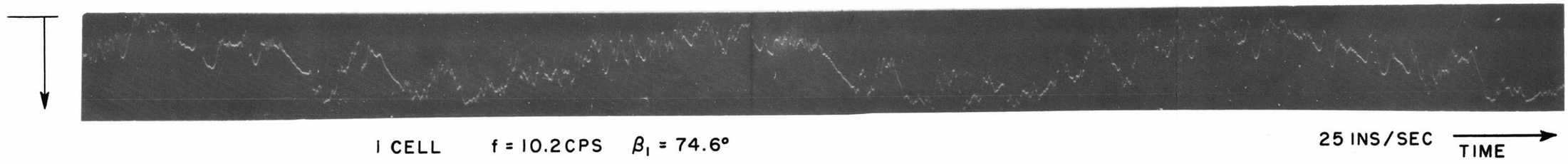

1 CELL f = 10.2 CPS $\beta_1 = 74.6°$ 25 INS/SEC TIME

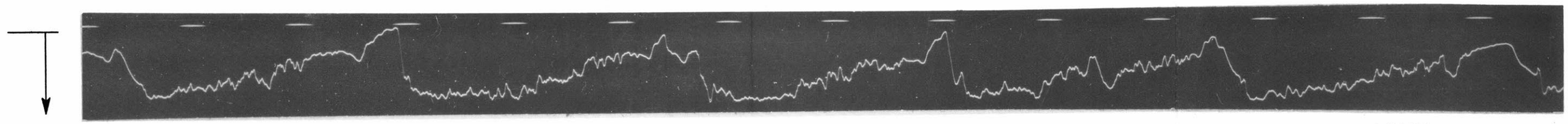

3 CELLS f = 38.5 CPS $\beta_1 = 79.4°$ PULSE = 100 CPS 100 INS/SEC TIME

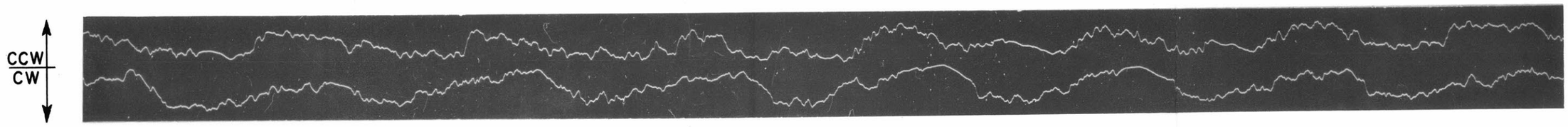

4 CELLS f = 52.0 CPS $\beta_1 = 84.9°$ 100 INS/SEC TIME

FIG. 5 REPRESENTATIVE STRIP FILM RECORDS OF HOT WIRE TRACES WITHOUT STATOR BLADES

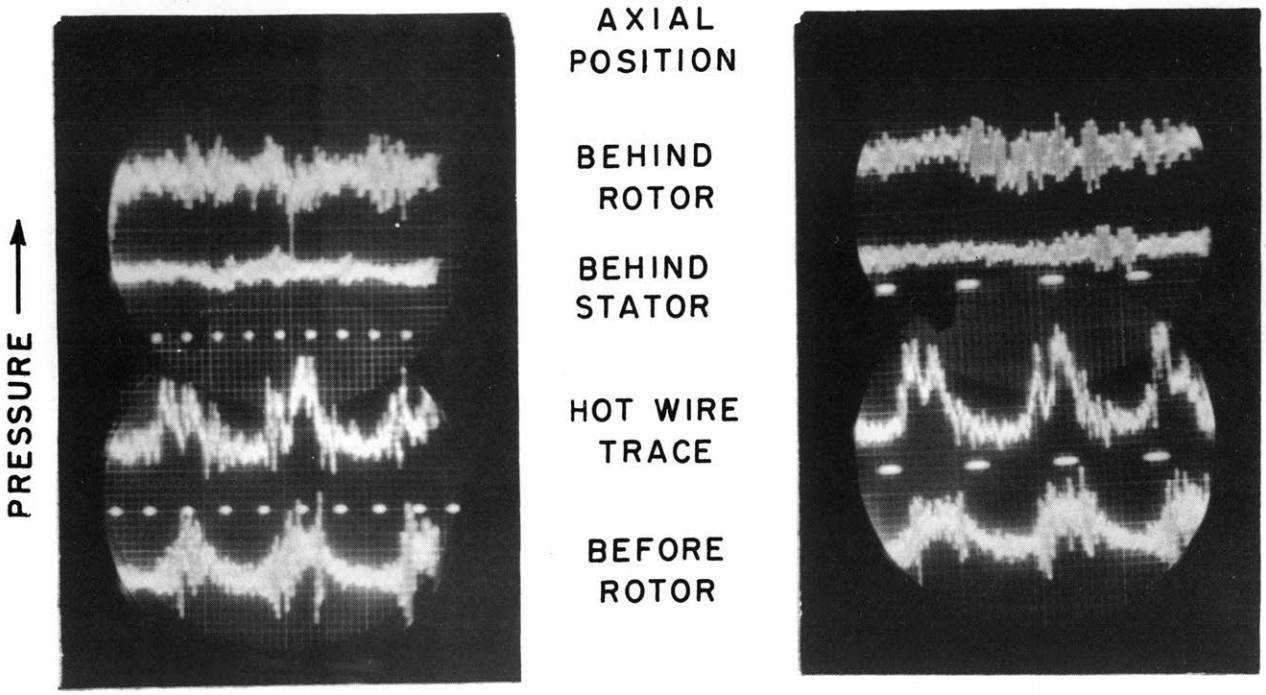

a. 1 CELL

b. 2 CELLS

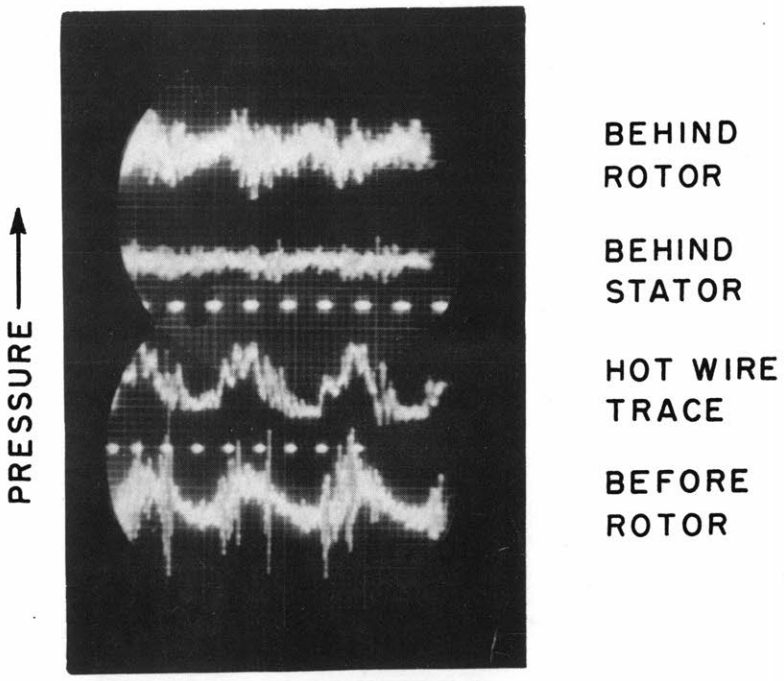

c. 3 CELLS

THE HOT WIRE TRACE IS ADDED FOR COMPARISON

FIG. 6 STATIC PRESSURE FLUCTUATIONS WITH STATOR BLADES

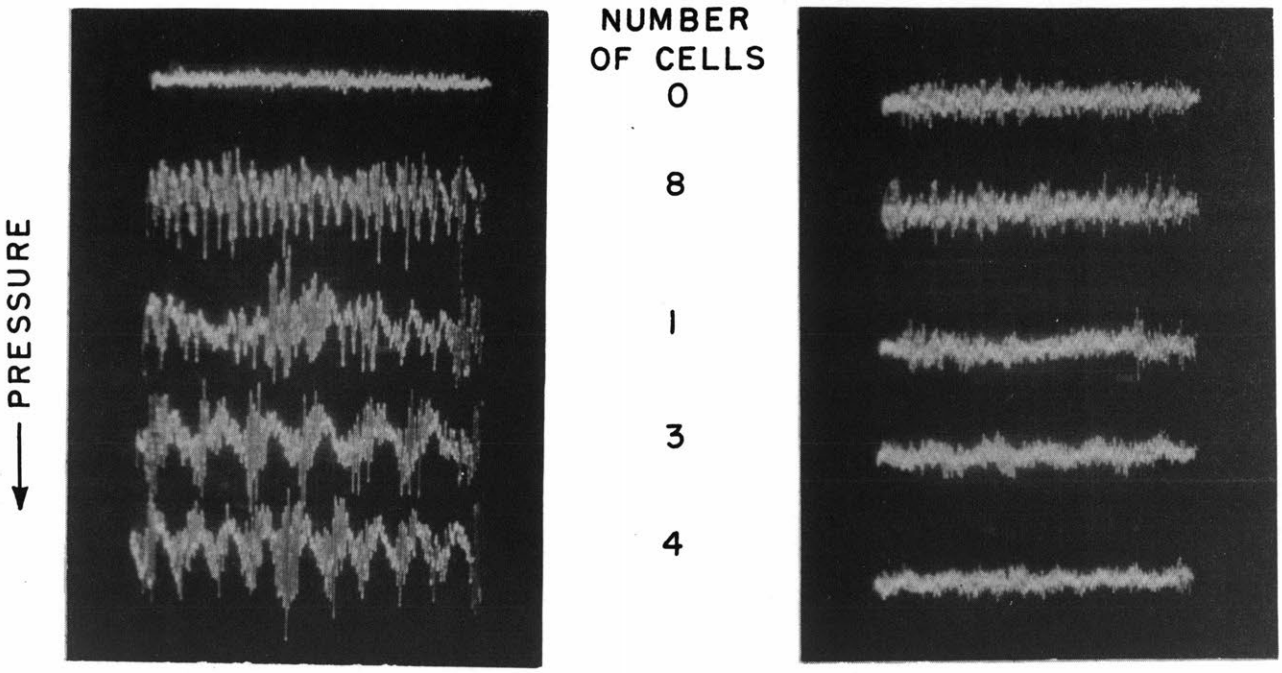

FIG. 7 STATIC PRESSURE FLUCTUATIONS WITHOUT STATOR BLADES

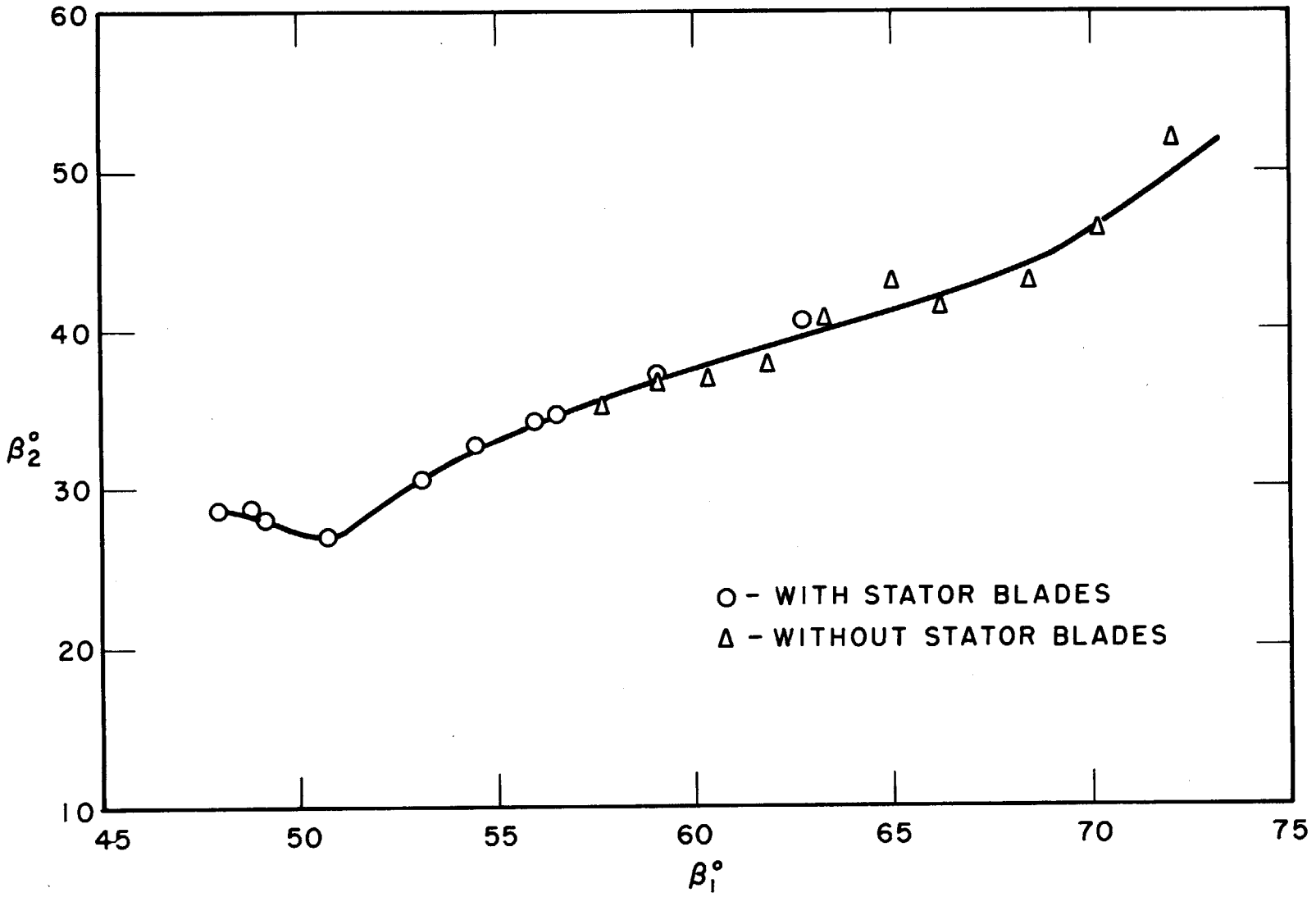

FIG. 8 ROTOR PERFORMANCE, β_2° VS β_1°

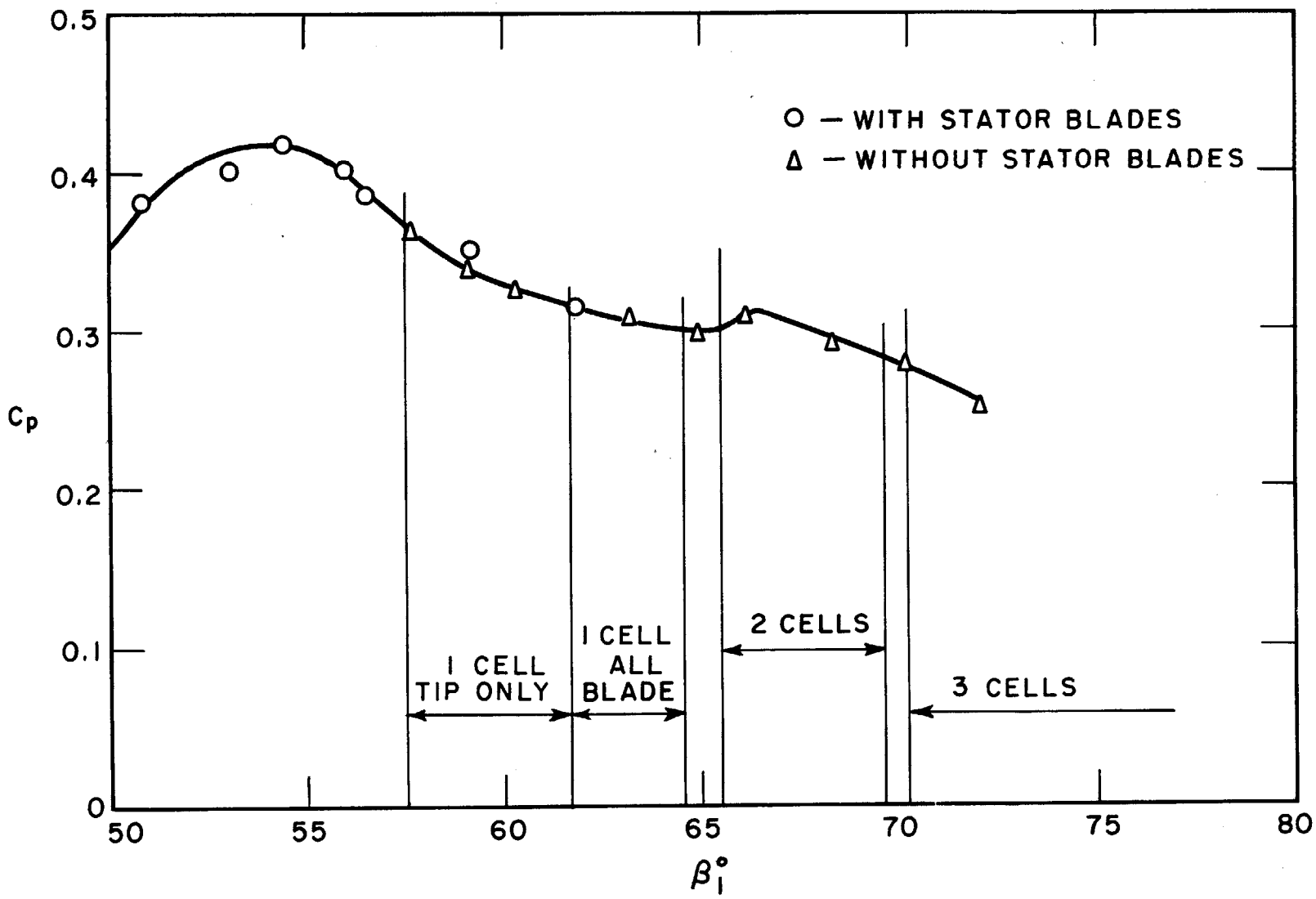

FIG. 9 ROTOR PERFORMANCE C_p VS β_1° SHOWING STALL REGIONS WITH STATOR BLADES.

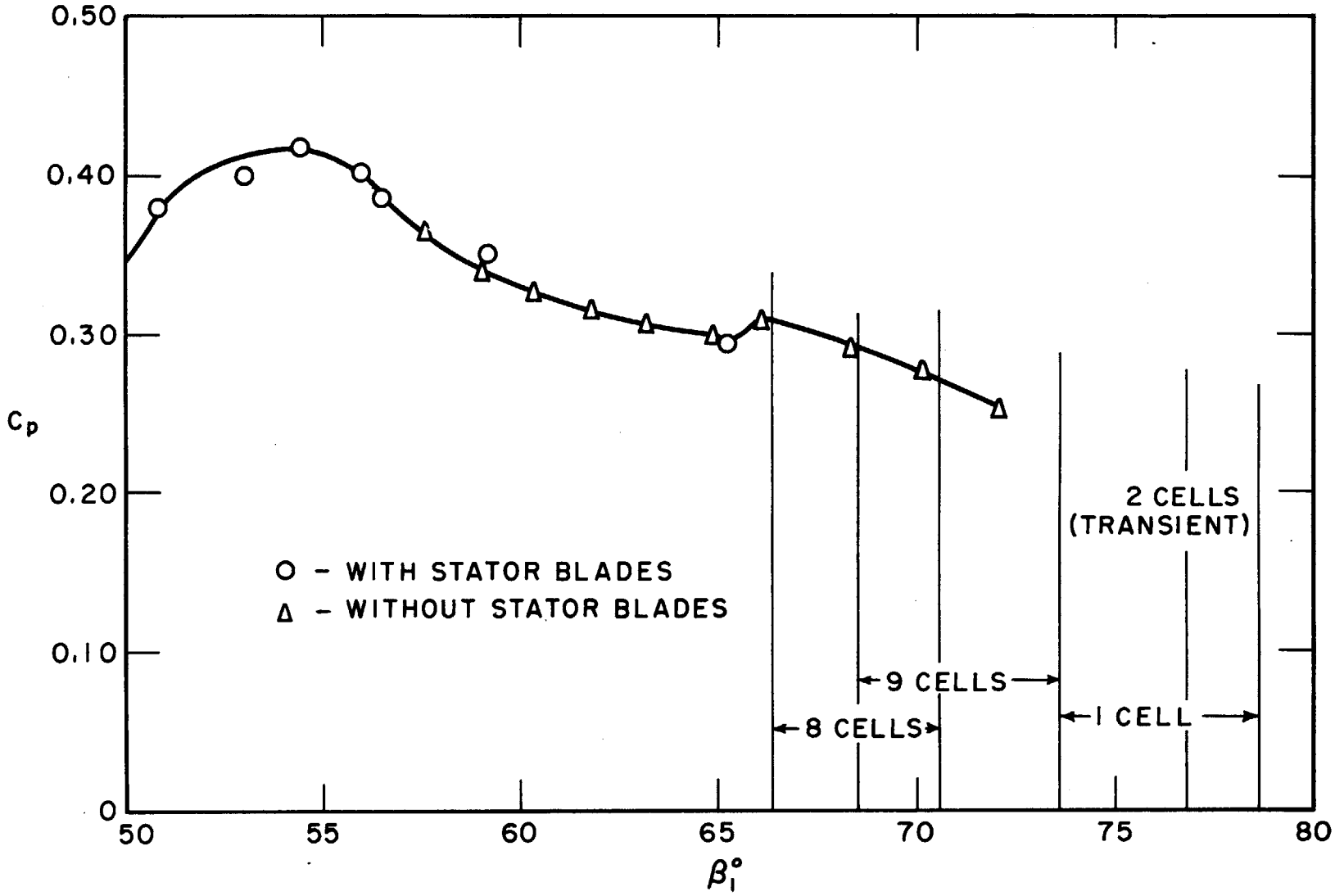

FIG. 10.- ROTOR PERFORMANCE C_p VS. β_1° SHOWING STALL REGIONS WITHOUT STATOR BLADES.

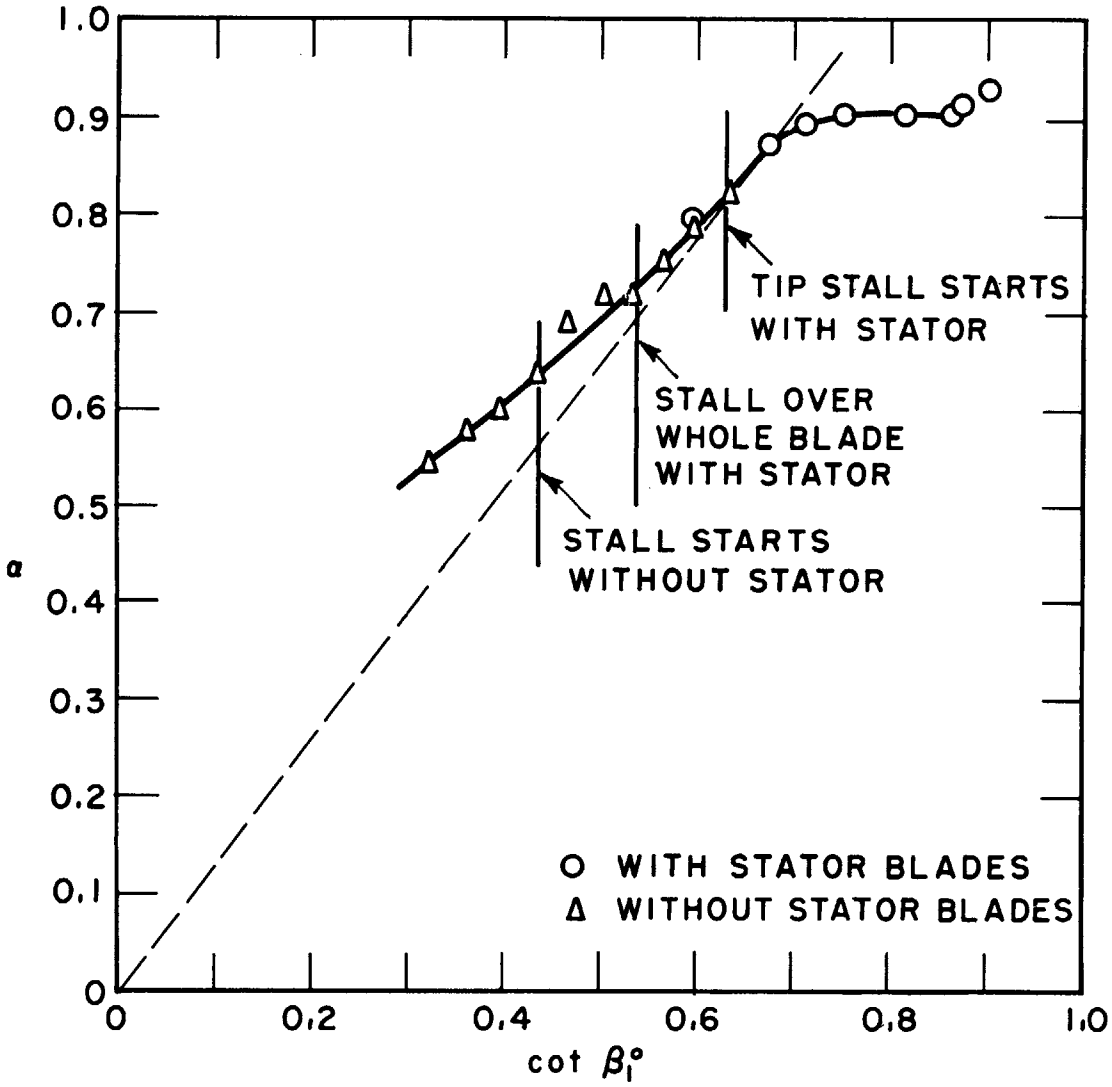

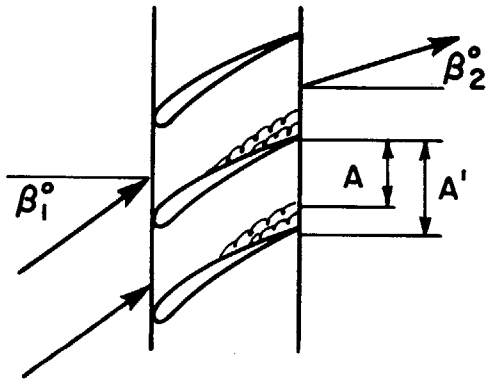

$$a \approx A/A' = \frac{\cos \beta_1^\circ}{\cos \beta_2 \sqrt{1-C_p}}$$

FIG. 11 BLOCKAGE COEFFICIENT · a VS $\cot \beta_1^\circ$

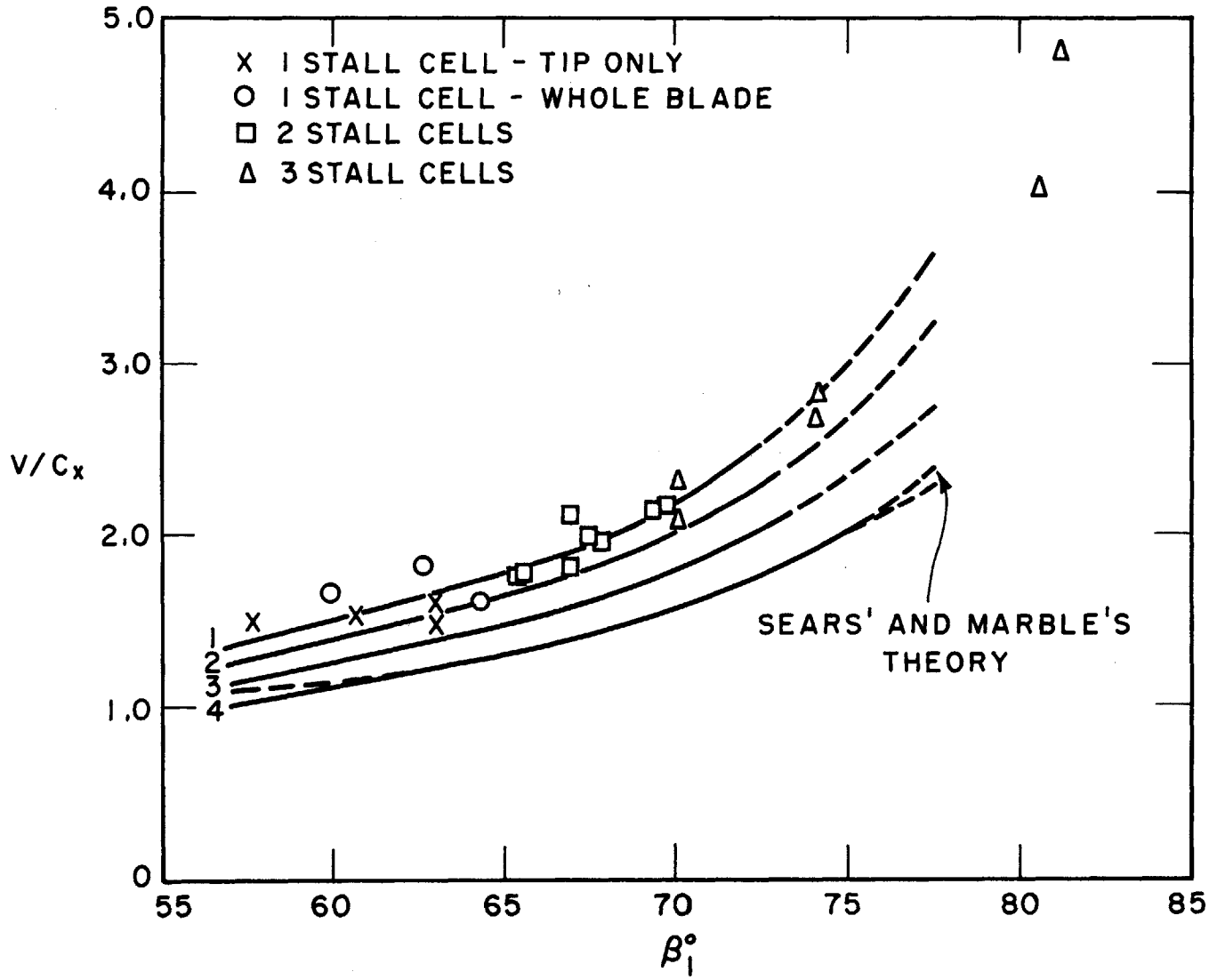

FIG. 12 - STALL PROPAGATION VELOCITIES V/C_x VS β_1° - WITH STATOR BLADES.

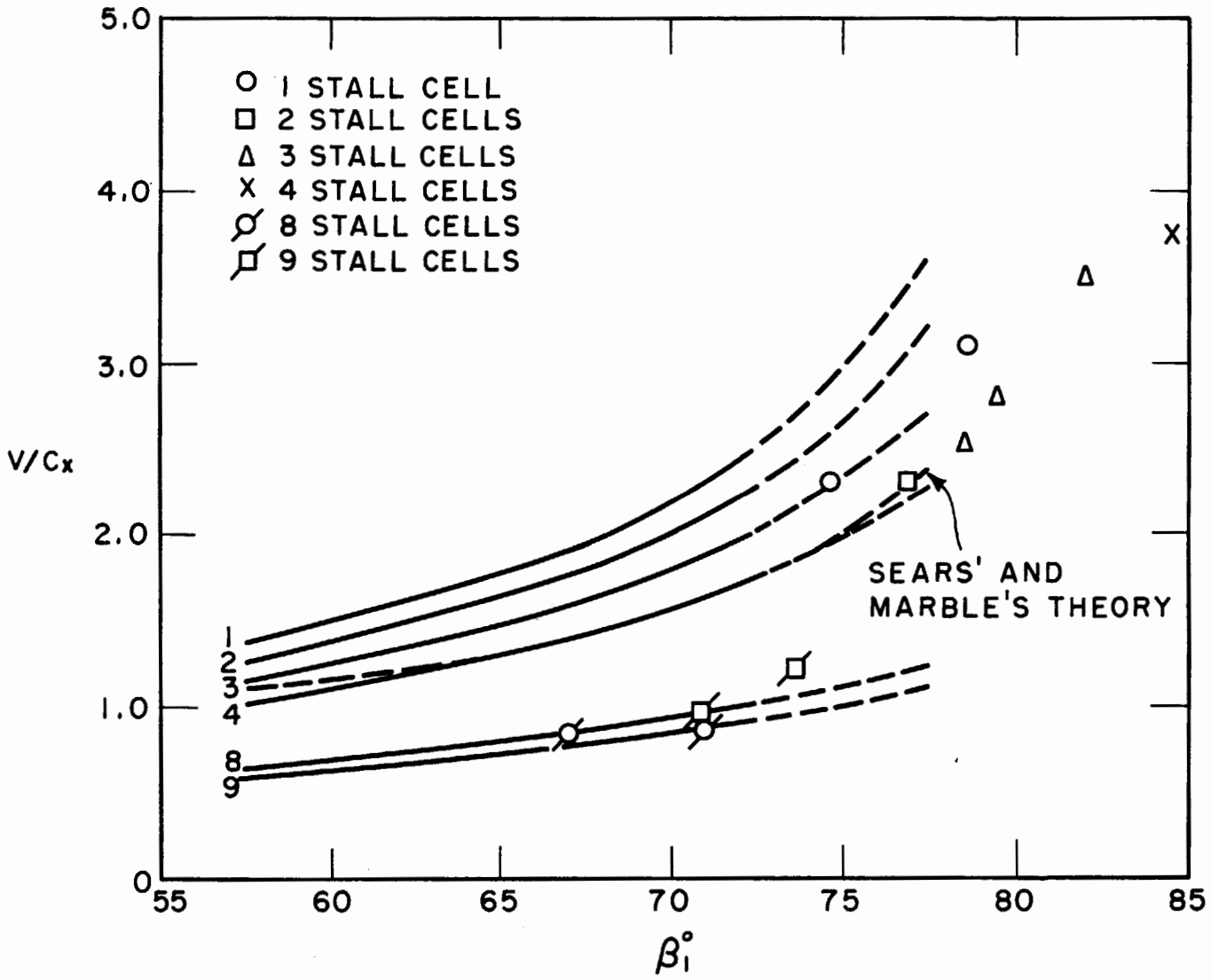

FIG. 13 STALL PROPAGATION VELOCITIES, V/C_x VS β_1° – WITHOUT STATOR BLADES.